Publications of the Astronomical Society of the Pacific, 128:104301 (10pp), 2016 October doi:10.1088/1538-3873/128/968/104301

Assessing the Structure of Isotropic and Anisotropic Turbulent Magnetic Fields

Marco Fatuzzo[1], Lisa Holden[2], Lindsay Grayson[2], and Kirk Wallace[2]
[1] Department of Physics, Xavier University, Cincinnati, OH 45207, USA
[2] Department of Mathematics and Statistics, Northern Kentucky University, Highland Heights, KY 41099, USA
Received 2016 February 5; accepted 2016 May 31; published 2016 September 5

Abstract

Turbulent magnetic fields permeate our universe, impacting a wide range of astronomical phenomena across all cosmic scales. A clear example is the magnetic field that threads the interstellar medium (ISM), which impacts the motion of cosmic rays through that medium. Understanding the structure of magnetic turbulence within the ISM and how it relates to the physical quantities that characterize it can thus inform our analysis of particle transport within these regions. Toward that end, we probe the structure of magentic turbulence through the use of Lyapunov exponents for a suite of isotropic and nonisotropic Alfvénic turbulence profiles. Our results provide a means of calculating a "turbulence lengthscale" that can then be connected to how cosmic rays propagate through magentically turbulent environments, and we perform such an analysis for molecular cloud environments.

Key words: cosmic rays – ISM: general – ISM: magnetic fields – magnetohydrodynamics (MHD)

1. Introduction

The propagation of high-energy cosmic rays through the interstellar medium (ISM) constitutes a fundamental process in astronomy and astrophysics. While our understanding of this subject has advanced significantly since the pioneering works of Jokipii (1966) and Kulsrud & Pearce (1969), the exact nature of particle transport through the turbulent magnetic fields that thread the ISM has yet to be determined.

A standard approach to this problem entails obtaining solutions to the diffusion equation. Although doing so generally requires numerical techniques, analytic solutions have been obtained for ideal scenarios (e.g., Atoyan et al. 1995; Aharonian & Atoyan 1996). Regardless, the complexities of the particle-field interactions are captured through an energy dependent diffusion coefficient (or coefficients for a non-isotropic medium) that are often informed by theoretical analyses. More recent theoretical treatments of cosmic-ray diffusion have benefitted from advances in our understanding of magnetic turbulence. While it is generally understood that turbulence is driven from a cascade of longer wavelengths to shorter wavelengths as a result of wave-wave interactions, obtaining a complete theory of MHD turbulence in the ISM has proven challenging. Complicating the issue, magnetic fluctuations decorrelate due to nonlinear interactions before they can propagate over distances of multiple wavelengths (Goldreich & Sridhar 1995)—an effect that leads to resonance broadening and as such, influences how thermal particles interact with turbulence (Lynn et al. 2012, 2013). Nevertheless, both theoretical investigations (e.g., Goldreich & Sridhar 1995; Lazarian & Vishniac 1999) and numerical simulations (e.g., Cho & Vishniac 2000; Cho & Lazarian 2003) have provided scaling laws that can then inform cosmic-ray diffusion theory (Yan & Lazarian 2002, 2004, 2008; Lazarian & Yan 2014).

Alternatively, it is now computationally viable to perform detailed numerical simulations of the diffusion process. Specifically, one can numerically integrate the equations of motion for a large ensemble of particles moving through a specified turbulent magnetic field in order to build up the particle distribution function at various times (e.g., Casse et al. 2002; O'Sullivan et al. 2009; Fatuzzo et al. 2010; Fatuzzo & Melia 2012). As with most treatments of cosmic-ray diffusion, the central issue to resolve with this approach is how to prescribe the magnetic field. Pioneering such efforts, Giacalone & Jokipii (1994) developed a formalism for generating a turbulent magnetic field $\delta\boldsymbol{B}$ as the superposition of a large number N of randomly polarized transverse static waves with wavelengths $\lambda_n = 2\pi/k_n$, where the corresponding magnitudes of the wavevectors are logarithmically spaced between $k_1 = 2\pi/\lambda_{\max}$ and $k_N = 2\pi/\lambda_{\min}$. Adopting a static turbulent field removes the necessity of specifying a dispersion relation between the wavevectors k_n and their corresponding angular frequencies ω_n. This approach appears suitable for considering highly nonlinear turbulence ($\delta B \gg B_0$), and can be extended to an environment without a background field B_0. Of course, turbulent magnetic fields in cosmic environments are not static. Nevertheless, a static formalism in spatial diffusion calculations of relativistic particles seems justified for environments in which the Alfvén speed (v_A) is much smaller than the speed of light. That is, since relativistic particles have speeds that are much greater than the Alfvén speeds expected throughout the ISM, their interaction with the turbulent fields should not be sensitive to dynamical processes that occur on MHD timescales.

In contrast, calculating the energy diffusion of particles through turbulent fields resulting from stochastic acceleration in the presence of electric field fluctuations does require a self-consistent way of incorporating Faraday's law into the formalism. Toward that end, O'Sullivan et al. (2009) extended the work of Giacolone & Jokipii to include the presence of electric fields in a dynamic magenetic field. In so doing, these authors replaced the waveforms of Giacolone & Jokipii with Alfénic waves, and used linear MHD theory to obtain dispersion relations for each wave. It should be noted that both the Giacolone & Jokipii and the O'Sullivan et al. treatements of the magnetic field produce the same results for spatial diffusion in the limit that $v_A \ll c$ (Fatuzzo & Melia 2012).

The aforementioned formalisms for prescribing magnetic turbulence are isotropic in that the directions of the wavevectors $\boldsymbol{k}_n$ are randomly selected in a spherically symmetric way. However, theorertical and numerical investigations in the past two decades indicate that the cascade from strong MHD turbulence in a uniform medium seemingly produces eddies on small spatial scales that are elongated in the direction of the underlying magnetic field, so that the components of the wave vector along ($k_{||}$) and across ($k_\perp$) the underlying field direction are related by the expression $k_{||} \propto k_\perp^{2/3}$ (Goldreich & Sridhar 1995; Cho & Vishniac 2000). Further, the cascade produces an energy spectrum that scales as $k_\perp^{-5/3}$ (Cho & Lazarian 2003). Motivated by this result, Fatuzzo & Melia (2014) modified the formalism of their previous works to develop a model for an anisotropic turbulent field in order to determine how energy diffusion would be affected, but did not focus on spatial diffusion. Taking a different approach, Xu & Yan (2013) obtained scattering and spatial diffusion coefficients by tracing particle trajectories through isothermal compressible MHD turbulence generated at 512^3 resolution via the numerical simulations presented in Cho & Lazarian (2003).

Clearly, there are now several different prescriptions for how to model the turbulent fields that appear in the recent literature. The goal of this paper is to compare several isotropic and anisotropic analytic turbulent magnetic structures through their Lyapunov exponents. The motivations for doing so are three-fold: (1) to determine the number of terms needed to suitably represent a turbulent field using a discrete methodology; (2) to gain insight as to how the structure of turbulent magnetic fields depends on the physical parameters that characterize them; and (3) to connect measures obtained from our analysis to the diffusion of particles through turbulent fields with the aim of informing numerical investigations of diffusion processes.

The paper is organized as follows. We present a standard analytic model for turbulent magnetic fields in Section 2, considering both isotropic and anisotropic cases. We characterize the turbulent structure of the magnetic fields for several turbulent profiles in Section 3, and connect our results to the diffusion of particles through those fields in Section 4. We apply our results to the special case of molecular cloud environments in Section 5, and summarize our results in Section 6.

2. An Analytic Model for Turbulent Magnetic Fields

To keep the analysis as straight-forward as possible, we treat the ISM as a nonviscous, perfectly conducting fluid threaded by a uniform, static magnetic field $\boldsymbol{B}_0 = B_0\hat{z}$. Although turbulence in the ISM is not well-understood, we make use of the accepted notion that energy is transferred from longer wavelengths to shorter wavelengths in a cascading fashion through wave-to-wave interactions, and model the net turbulent field as the superposition of N randomly polarized transverse waves. We consider the field structure at some instant in time, removing the necessity of specifying a dispersion relation between the wavevectors k_n and their corresponding angular frequencies ω_n. The turbulent field is therefore given by the static expression

$$\delta\boldsymbol{B} = \sum_{n=1}^{N} \boldsymbol{A}_n \, e^{i(\boldsymbol{k}_n\cdot\boldsymbol{r}+\beta_n)}, \tag{1}$$

where the wavevectors have magnitudes that are logarithmically spaced between $k_1 = 2\pi/\lambda_{\max}$ and $k_N = 2\pi/\lambda_{\min}$ (e.g., Giacalone & Jokipii 1994; Casse et al. 2002; Fatuzzo et al. 2010). Suitable values for N are determined in Section 3 by examining the Lyapunov exponents of the turbulent fields.

For our calculations, we focus primarily on large amplitude turbulence, which we quantify through the ratio of the energy density of the magnetic field to that of the background static field via the parameter

$$\eta \equiv \frac{\langle \delta B^2 \rangle}{B_0^2}. \tag{2}$$

Specifically, we consider primarily scenarios for which $\eta = 1$, but also present limited results for small amplitude turbulence ($\eta \ll 1$). We also consider both the isotropic case and the perhaps more realistic anisotropic scenario in the large amplitude turbulence limit for Kolmogorov turbulence (as detailed below).

For the isotropic case, the direction of each propagation vector $\boldsymbol{k}_n$ is set through a random choice of coordinate angles θ_n and ϕ_n, and the phase of each wave is set through a random choice of β_n. The appropriate choice of Γ in the scaling

$$A_n^2 = A_1^2 \left[\frac{k_n}{k_1}\right]^{-\Gamma} \frac{\Delta k_n}{\Delta k_1} = A_1^2 \left[\frac{k_n}{k_1}\right]^{-\Gamma+1} \tag{3}$$

sets the desired spectrum of magnetic turbulence (e.g., $\Gamma = 1$ for Bohm, $3/2$ for Kraichnan and $5/3$ for Kolmogorov turbulence). Note that the value of $\Delta k_n/k_n$ is the same for all n due to our logarithmic binning scheme. The strength of the turbulent magnetic field, η, sets the value of A_1, such that

$$A_1^2 = \frac{\eta B_0^2}{\sum_{n=1}^{N}\left(\frac{k_n}{k_1}\right)^{\Gamma-1}}. \tag{4}$$

For the anisotropic case, the cascade from longer to shorter wavelenghts is expected to produce eddies on small spatial scales that are elongated in the direction of the underlying static magnetic field (Goldreich & Sridhar 1995; Cho & Lazarian 2003). As such, the direction of each perpendicular wavevector $k_{n\perp}$ is set through a random choice of azimuthal angle ϕ_n, and the phase of each term is again set through a random choice of β_n. The corresponding parallel component of the wavevector is given by

$$k_{n||} = \pm\frac{\sqrt{2}}{2} k_{1\perp}^{1/3}\, k_{n\perp}^{2/3} \tag{5}$$

(with a randomly chosen sign), such that

$$k_1 = \sqrt{k_{1\perp}^2 + k_{1||}^2} = \frac{2\pi}{\lambda_{\max}}. \tag{6}$$

Guided by Goldreich & Sridhar (1995), we only consider a Kolmogorov-like profile for the nonisotropic case, so that

$$A_n^2 = A_1^2\left[\frac{k_{n\perp}}{k_{1\perp}}\right]^{-5/3+1}, \tag{7}$$

but we note that the spectrum of fluctuations in the direction parallel to the local magnetic field is not Kolmogorov but corresponds to k^{-2}.

Alfvén waves are transverse waves, thus their fluid velocity $\boldsymbol{v}$ satisfies the condition $\boldsymbol{k}\cdot\boldsymbol{v} = 0$. In addition, the fluid velocity is perpendicular to the underlying static magnetic field. The fluid velocity associated with the nth term in Equation (1) is then given by

$$\delta\boldsymbol{v}_n = \pm A_n \frac{v_A}{B_0}\frac{\boldsymbol{B}_0\times\boldsymbol{k}_n}{|\boldsymbol{B}_0\times\boldsymbol{k}_n|}\, e^{i(\boldsymbol{k}_n\cdot\boldsymbol{r}+\beta_n)}, \tag{8}$$

where the sign is chosen randomly for each term in the sum. Each wave thus has a magnetic field given by the linear form of Ampère's Law,

$$\boldsymbol{A}_n = \mp A_n \frac{\boldsymbol{k}_n\cdot\boldsymbol{B}_0}{|\boldsymbol{k}_n\cdot\boldsymbol{B}_0|}\frac{\boldsymbol{B}_0\times\boldsymbol{k}_n}{|\boldsymbol{B}_0\times\boldsymbol{k}_n|}, \tag{9}$$

matching the fields given by O'Sullivan et al. (2009).

We note that the turbulent magnetic fields in our formalism are functionally described through a particular choice of the five parameters B_0, $\lambda_{\max}$, $\lambda_{\min}$, η, and Γ. However, since all spatial quantities are easily scaled to $\lambda_{\max}$, and the field strength is easily scaled to B_0, one need only define the following three parameters in order to specify a turbulent field profile: $d \equiv \lambda_{\max}/\lambda_{\min}$, η, and Γ. A realization of a given profile is then generated through the particular choice of the random variables (e.g., θ_n, β_n). Of course, one must also address the issue of how many terms per decade in k space must be incuded in the sum to suitably represent a continuous structure. We will focus on this issue in the next section.

3. The Structure of Magnetic Turbulence

In order to investigate the structure of the turbulent magnetic fields, we borrow an idea from chaos theory and compute the Lyapunov spectrum that characterizes the lengthscale on which two initially nearby field lines diverge from each other. Applying this idea to our problem, we imagine an infinitesimal sphere in space containing "initial conditions" that follow their respective field lines over some distance s. As a result, this sphere will deform, evolving into an ellipsoid with principal axes that rank from most rapidly to least rapidly growing.

Since the structure exists in three spatial dimensions, there will be three principle axes (but note that they are not "fixed" along spatial directions), and hence, three Lyapunov exponents. In addition, the system is conservative, so the volume element of the phase space will be the same along a trajectory. In turn, the sum of the Lyapunov exponents must be zero. A turbulent field structure will therefore be charactertized by a Lyapunov spectrum of the form (λ_L, 0, λ_{-L}), where $\lambda_L > 0$ characterizes the average rate of divergence of nearby field lines through an expression of the form

$$|\delta\boldsymbol{r}(s)| = |\delta\boldsymbol{r}(0)|\, e^{\lambda_L s}. \tag{10}$$

In this equation, $\delta\boldsymbol{r}(0)$ represents an initial displacement vector between two points on nearby field lines, and $\delta\boldsymbol{r}(s)$ represents the ensuing displacement vector as the two points each advance along their respective field lines a distance s (as illustated in Figure 1). As elaborated on below, the value of $1/\lambda_L$ represents the distance along a fieldline that must be traversed before information regarding an initially neighboring fieldline is lost. But it is important to note that although Lypunov exponents measure how two nearby points move apart as a function of distance as they travel along their respective field line, any divergence that occurs on small scales will not persist for larger scales (this is true even for the Lorentz attractor). This point will be expanded on further at the end of this section.

We begin by exploring the structure of an isotropic turbulent field defined through the baseline parameters $\Gamma = 5/3$, $\eta = 1$, and $d = 10^4$ (Profile 1), adopting a value of $N_d \equiv N/\log_{10}(d) = 20$ terms per decade in k space. The Lyapunov spectrum is calculated using the formalism described in Wolf et al. (1985). Figure 1 shows how two fieldlines with our baseline profile diverge from each other from their initial nearby locations. Figure 2 then shows the Lyapunov spectrum calculated as a function of s for one of these field lines. Note that the Lyapunov

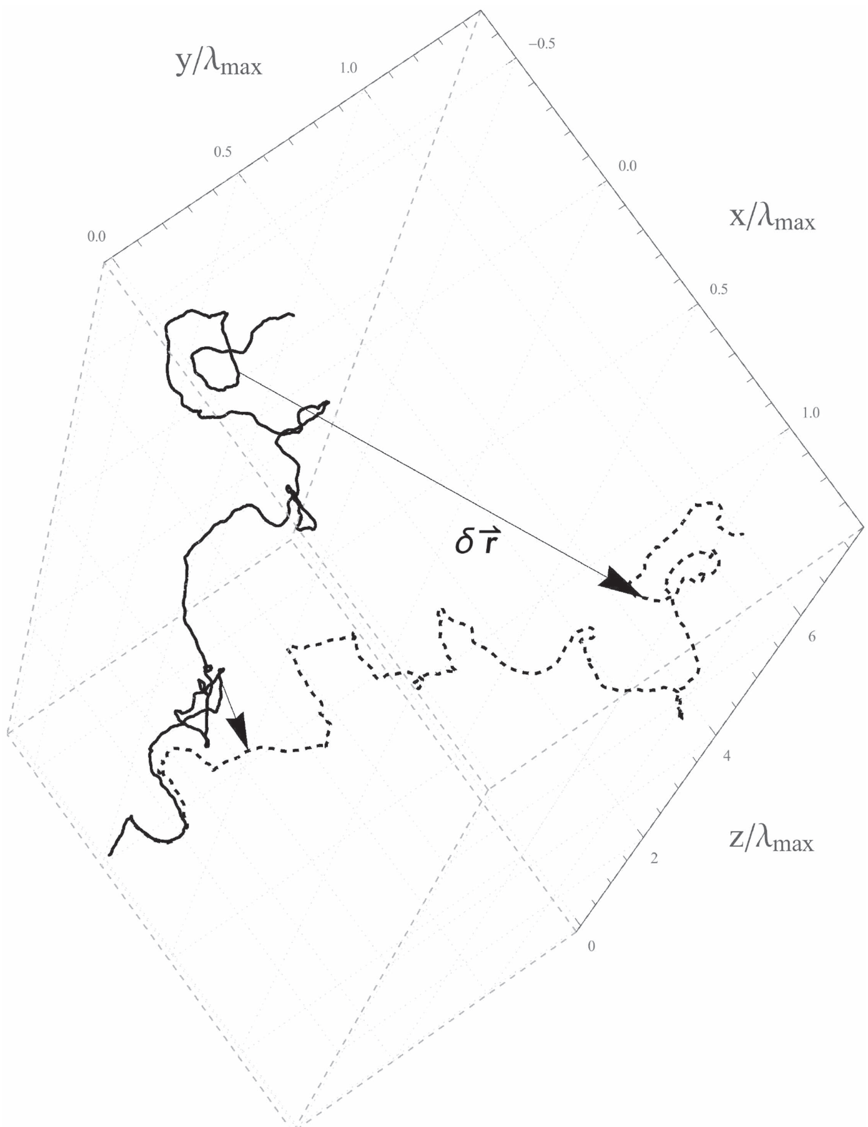

Figure 1. Two field lines, one that crosses the origin (which defines its value of $s = 0$), and the other that is separated from the first by a displacement $\delta \boldsymbol{r}(0) = 10^{-6}\lambda_{\max}\hat{x}$ at its value of $s = 0$. The two arrows represent the displacement vectors between points on these field lines at two different values of s. The divergence of these displacement vectors is characterized by the positive Lyapunov exponent.

exponents are calculated as a running sum, and therefore need to settle to their asymptotic values. Our results indicate that an asymptotic value is reached for a distance of $s \gtrsim 30\lambda_{\max}$, for which the turbulent structure of the field has been sufficiently sampled (though for certain profiles, the settling distance can be considerably greater).

For a discrete treatment of a turbulent field, the value of λ_L is sensitive to the specific realization of a field profile (that is, on the specific values of the random variables used to set the directions of each wavevector $\boldsymbol{k}_n$). As such, the turbulent structure of a given field profile is characterized by a distribution of λ_L values generated by sampling over many realizations of that profile. Throughout this work, we sample 200 realizations of each turbulent field profile in order to build up meaningful distributions. The results for our baseline profile is shown in Figure 3. As can be seen, the distribution is relatively well-fit by a Gaussian curve, and we therefore use the mean $\langle\lambda_L\rangle$ and standard deviation σ_λ of the distributions obtained to characterize each profile.

From this baseline case, we explore how the magnetic structure depends on each of the three turbulent field parameters (Γ, η, d) through a numerical invesigation of 10

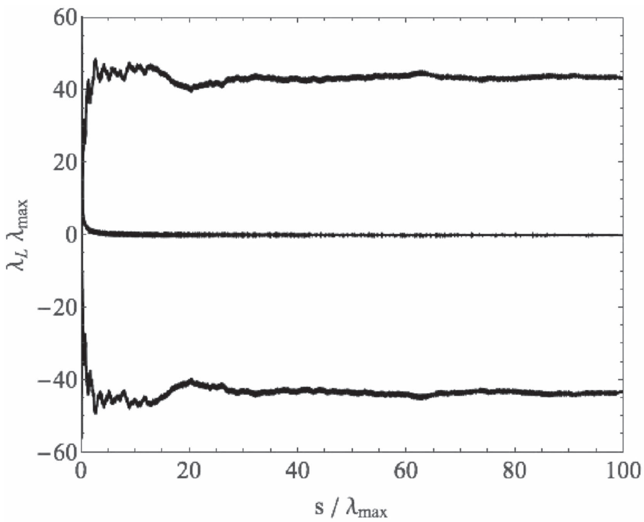

Figure 2. The running average of the Lyapunov exponents calculated for one realization of a turbulent magnetic field characterized by $\Gamma = 5/3$, $\eta = 1$, and $d = 10^4$ (our baseline profile). The value of λ_L (in units of $1/\lambda_{max}$) settles down to its asymptotic value once $s \gtrsim 30\lambda_{max}$.

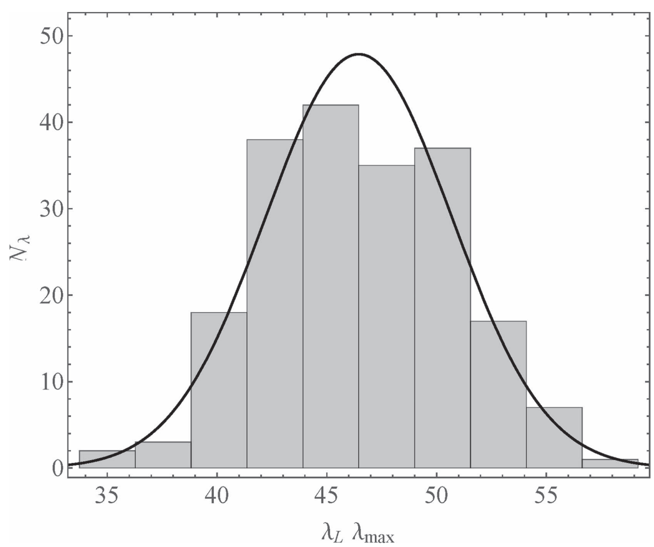

Figure 3. The distribution of positive Lyapunov values (in units of $1/\lambda_{max}$) for 200 realizations of our baseline turbulent field profile ($\Gamma = 5/3$, $\eta = 1$, $d = 10^4$). The solid curve shows a Guassian fit with the same mean and standard deviation as the distribution shown.

Table 1
Summary of Experiments

Pr.	Γ	η	d	λ_{Li}	σ_i/λ_{Li}	λ_{La}	σ_a/λ_{La}
1	5/3	1	10^4	46	0.09	22	0.06
2	3/2	1	10^4	115	0.11	…	…
3	1	1	10^4	1160	0.13	…	…
4	5/3	0.3	10^4	24	0.14	…	…
5	5/3	10^{-1}	10^4	10	0.20	…	…
6	5/3	10^{-2}	10^4	1.1	0.47	…	…
7	5/3	10^{-3}	10^4	0.095	1.0	…	…
8	5/3	1	10^3	19.3	0.10	12	0.06
9	5/3	1	10^2	7.3	0.10	6.1	0.07
10	5/3	1	10	2.6	0.12	2.5	0.09

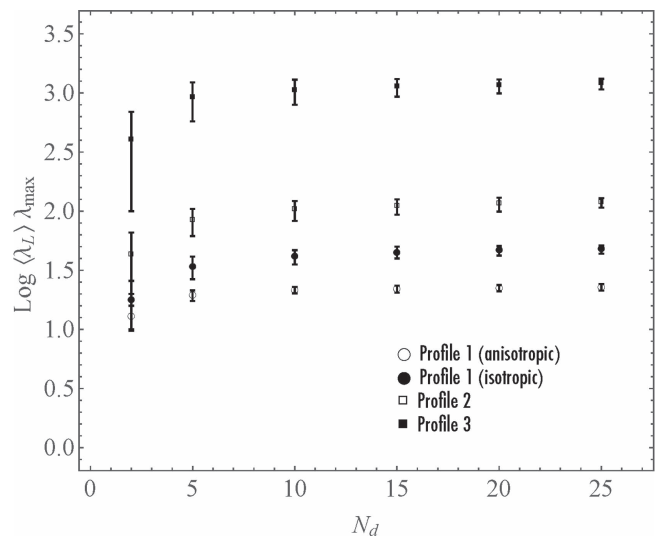

Figure 4. Mean values of the distributions of positive Lyapunov exponents calculated for profiles 1–3, but with different values of N_d (terms per decade). Open circles—anisotropic turbulence with $\Gamma = 5/3$, $\eta = 1$, $d = 10^4$; solid circles—isotropic turbulence with $\Gamma = 5/3$, $\eta = 1$, $d = 10^4$; open squares—isotropic turbulence with $\Gamma = 3/2$, $\eta = 1$, $d = 10^4$; solid sqaures—isotropic turbulence with $\Gamma = 1$, $\eta = 1$, $d = 10^4$. Error bars represent 1-σ_λ values.

isotropic profiles and 4 anisotopic profiles, as defined in Table 1 (with i and a subscripts representing isotropic and anisotropic cases, respectively). Lyapunov exponents are calculated for 200 realizations of each profile, and the means and standard deviations of each resulting distribution are then tabulated. To justify the use of $N_d = 20$ terms per decade adopted throughout our analysis as a suitable choice for modeling a continuous magnetic structure using a discrete sum of terms, we also perform our analysis for Profiles 1–3 using the values of $N_d = 2$, 5, 10, 15 and 25. The corresponding results, presented in Figure 4, indicate that $\langle\lambda_L\rangle$ does not change appreciably once $N_d \gtrsim 5$.

In addition, since the structure of a continuous turbulent field should yield a unique value of λ_L, the ratio $\sigma_\lambda/\langle\lambda_L\rangle$ of the distribution obtained using a discrete treatment reflects, to some extent, how well the discrete formalism mimics a continuous turbulent profile. Indeed, the results shown in Figure 4 show that $\sigma_\lambda/\langle\lambda_L\rangle$ decreases as N_d increases, and is $\lesssim 0.15$ once $N_d \gtrsim 20$ for large amplitude turbulence. This result indicates that a discrete formalism with 20 terms per decade is expected

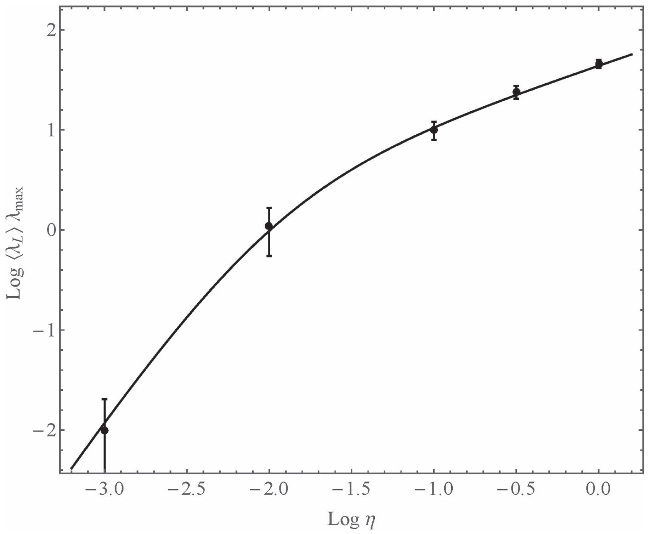

Figure 5. Mean values of the distributions of positive Lyapunov exponents calculated for profile 1(isotropic case) and profiles 4–7, which illustrate the dependence of $\langle\lambda_L\rangle$ on the turbulence strength as defined by the parameter η. Error bars represent 1-σ_λ values obtained from the distributions. The solid curve shows a fit to the data given by a split powerlaw, as given by the expression in Equation (11).

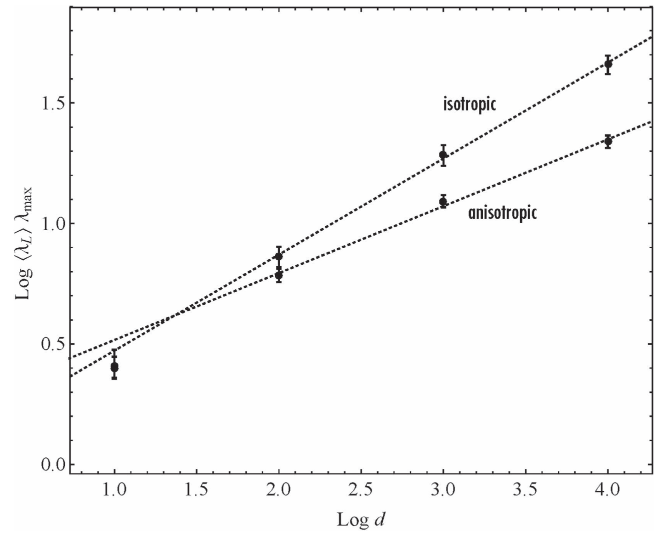

Figure 6. Mean values of the distributions of positive Lyapunov exponents calculated for both isotropic and anisotropic cases of profiles 1 and 8–10. The dashed lines represent fits to the data, but exclude the $d = 10$ data points. Error bars represent 1-σ_λ values obtained from the distributions.

to yield a magnetic field structure accurate to $\lesssim$15% of an ideal "continuous" structure for 67% of profile realizations, which in turn characterizes how well our choice of N_d describes a continuous turbulent magnetic field.

We now consider how the structure of an isotropic turbulent field depends on the type of tubulence profile, as defined by the index Γ. As can be seen from the results in Table 1, there is a strong dependence between Γ and $\langle\lambda_L\rangle$. This result is not surprising given that a smaller value of Γ corresponds to magnetic intensity being spread out more equitably across the full range of wavelengths, thus increasing the relative contribution of shorter wavelengths. Recalling that λ_L^{-1} represents the lengthscale over which neighboring fieldlines diverge, we define the turbulence lengthscale for a given profile as $s_T \equiv 1/\langle\lambda_L\rangle$, and find $s_T \approx 0.02\lambda_{\max}$ for isotropic Kolmogorov ($\Gamma = 5/3$) turbulence, $s_T \approx 0.05\lambda_{\max}$ for anisotropic Kolmogorov turbulence, $s_T \approx 0.009\lambda_{\max}$ for (isotropic) Kraichnan ($\Gamma = 3/2$) turbulence, and $s_T \approx 0.0009\lambda_{\max}$ for (isotropic) Bohm ($\Gamma = 1$) turbulence.

We next illsutrate in Figure 5 how the field structure depends on the strength of the turbulent field for Kolmogorov turbulence (Profiles 1 and 4–7 in Table 1). There is a strong dependence between $\langle\lambda_L\rangle$ and the turbulence strength parameter η, and the curvature exhibited by the data points indicate that the turbulence lengthscale increases more dramatically as η decreases. Indeed, the turbulence lengthscale increases from $\approx 0.1\lambda_{\max} \to \lambda_{\max} \to 100\lambda_{\max}$ as η decreases from $10^{-1} \to 10^{-2} \to 10^{-3}$ for the profiles shown in Figure 5. A good fit to the data is obtained by a split powerlaw of the form

$$\langle\lambda_L\rangle = \frac{2.2\times 10^5}{\lambda_{\max}}\,\frac{\eta^{2.4}}{(1+100\eta)^{1.85}}, \tag{11}$$

as shown by the solid curve in Figure 5.

Finally, we illustrate in Figure 6 how the dynamic range over which turbulence acts affects the Lyapunov exponents, focusing on large amplitude Kolmogorov turbulence as defined through profiles 1 and 8–10. Our results indicated that there is a clear dependence between $\langle\lambda_L\rangle$ and d for both isotropic and anisotropic turbulence, with the former well represented by the relation $\langle\lambda_L\rangle/\lambda_{\max} = 1.2\,d^{0.40}$, and the latter well represented by the relation $\langle\lambda_L\rangle/\lambda_{\max} = 1.7\,d^{0.28}$, though these fits do not include the $d = 10$ data points (including these data points noticably affects the quality of the fits). Our results show that isotropic profiles are characterized by larger Lyapunov coefficients and have a greater sensitivity to d than their anisotropic counterparts. This result is not surprising given that anisotropic turbulence prescribes the relation between $k_\perp$ and $k_{||}$, thus effectively reducing turbulence to a two-dimensional structure.

As noted above, Lypunov exponents measure how two nearby points move apart as a function of distance as they travel along their respective field line. But a positive Lyapunov exponent does not mean that a bundle of initially nearby field lines will diverge exponentially over large scales. As a way of illustrating this point, we first quantify the magnetic field wandering for the isotropic case of profile 1. Specifically, we follow 1000 fieldlines that cross the z axis at a randomly chosen point on a ring of radius $r_0 = 10^{-3}\,\lambda_{\max}$ centered on the origin

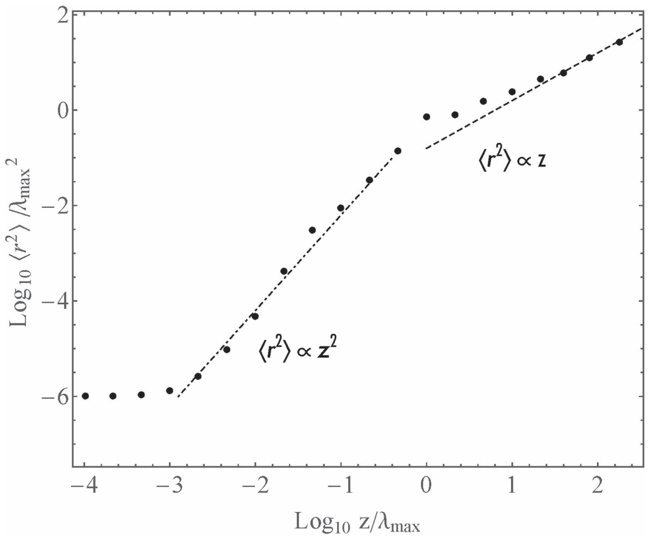

Figure 7. Magnetic field wandering for a bundle of 1000 field lines that cross the x–y plane randomly on a ring of radius $r_0 = 10^{-3}\,\lambda_{\max}$, where $r = \sqrt{x^2 + y^2}$ for each field line represents the "perpendicular" distance between that field line and the z-axis along which the unperturbed field $\boldsymbol{B}_0$ is directed. For reference, the dotted–dashed line scales as $\langle r^2 \rangle \propto z^2$, and the dashed line scales as $\langle r^2 \rangle \propto z$.

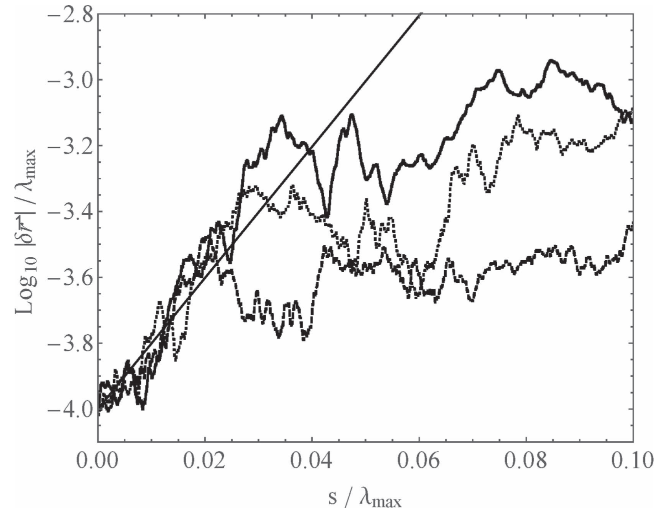

Figure 8. Magnitude of the displacement vector between initially nearby points that move along field lines a distance s for three different realizations of the isotropic case of profile 1. The solid line represents the expected separation as given by Equation (10), where $\lambda_L = 46/\lambda_{\max}$ was used based on the results of our experiments (see Table 1).

(and on the x–y plane). We then calculate the "perpendicular" distance ($r = \sqrt{x^2 + y^2}$) that each field line is from the z-axis at several different values of z, and calculate $\langle r^2 \rangle$ for each ensuing distribution (recall that the unperturbed field $\boldsymbol{B}_0 = B_0 \hat{z}$). Our results are presented in Figure 7, and are qualitatively similar to those presented in Beresnyak (2013; Figure 1). Note, however, that the power-law growth exhibited in our analysis at small scales goes as $\langle r^2 \rangle \propto z^2$ rather than $\langle r^2 \rangle \propto z^3$ for the anisotropic field structures considered by Beresnyak (see also Lazarian & Vishniac 1999; Lazarian & Yan 2014).

To try and reconcile this global field behavior with the use of Lyapunov exponents as measures for the turbulent magnetic fields presented in our work, we next consider how two nearby points move with respect to each other as they advance along their respective field lines a distance s. Specifically, we calculate the magnitude of the displacement vector between the points as a function of field-length s for three different realizations of the isotropic case of profile 1. The initial separation in each case was taken to be $|\delta \boldsymbol{r}(0)| = 10^{-4}\lambda_{\max}$. Our results are shown in Figure 8. The solid line represents the expected separation as given by Equation (10), where $\lambda_L = 46/\lambda_{\max}$ was used based on the results of our experiments (see Table 1). Although the curves are quite jagged (as expected), they also follows the expected trendline as found through our analysis. Our results thus indicate that Lyapunov exponents do provide a useful measure of the field structure on small scales.

4. Particle Diffusion

The output measures used to characterize the magnetic structures in Section 3 should somehow connect to the transport of charged particles through said structures, and understanding that connection could be helpful in guiding diffusion calculations. Toward that end, we note that charged particle diffusion is a resonance phenomena wherein particles interact with the turbulent field on the same lengthscale as their radius of gyration, denoted here as R_g. As such, the diffusion of a particle through a turbulent magnetic field is only sensitive to the part of the turbulence spectrum with wavelength $R_g \lesssim \lambda \lesssim \lambda_{\max}$ (Fatuzzo et al. 2010). This result suggests that the field structure for a profile characterized by a given value of d is "probed" by particles with a radius of gyration $R_g \approx \lambda_{\max}/d$.

To test the validity of this claim, we perform a suite of experiments whereby the equations that govern the motion of relativistic charged particles through a turbulent magnetic field are numerically integrated for 200 different randomly injected particles, each sampling their own realization of a given field profile (see Fatuzzo et al. 2010 for a complete discussion of this process). The values of Γ and η for the turbulent field through which the particles diffuse are set according to the profile being probed, which then leaves for the particle energy to be set so that the particle radius of gyration through the underlying field B_0 is given by $R_g = \lambda_{\max}/d$ (where d is then the third parameter that defines a profile). As noted above, these

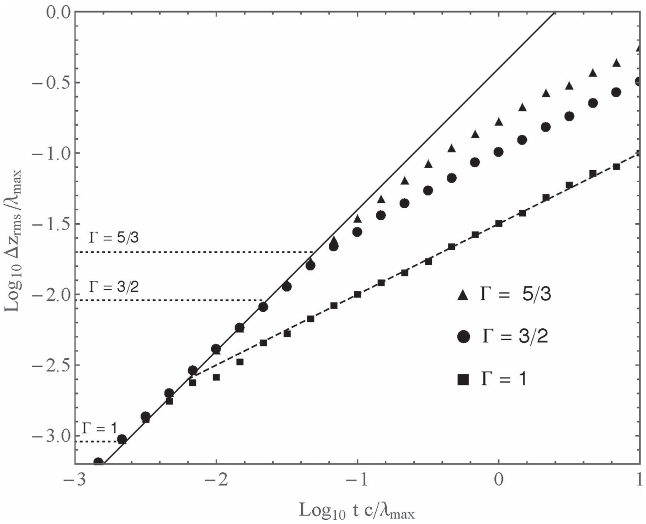

Figure 9. Root mean square values of the displacement Δz along the underlying field for an ensemble of particles injected into a turbulent (isotropic) magnetic field as defined by profiles 1–3 are plotted at the different times for which the distributions were calculated (with time given in terms of $c/\lambda_{\max}$). The solid line has slope 1 and the dashed line has slope $1/2$. The dotted horizontal lines represent the values of s_T for profiles with the denoted value of Γ.

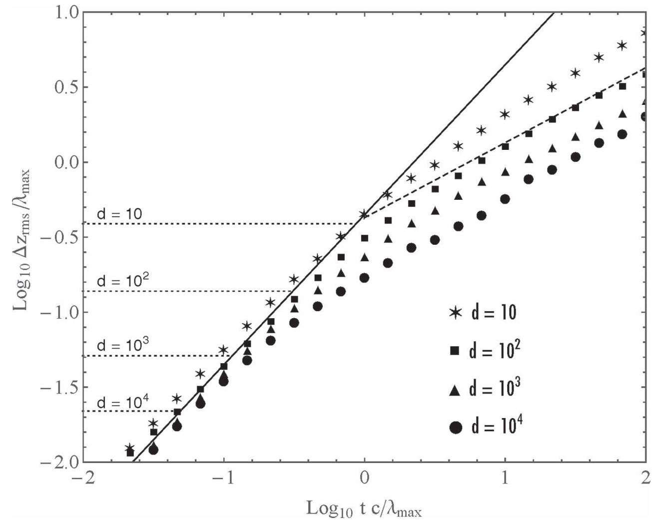

Figure 10. Root mean square values of the displacement Δz along the underlying field for an ensemble of particles injected into a turbulent (isotropic) magnetic field as defined by profiles 1 and 8–10 are plotted at the different times for which the distributions were calculated (with time given in terms of $c/\lambda_{\max}$). The solid line has slope 1 and the dashed line has slope $1/2$. The dotted horizontal lines represent the values of s_T for profiles with the denoted value of d.

particles thus experience the field turbulence over the range of wavelengths that spans between $\lambda_{\max}$ and $\lambda_{\max}/d$. The distributions of the displacement along the field direction is obtained at several different times for each profile, and the root mean square (rms) values ($\Delta z_{\rm rms}$) are then determined at each time.

Results are presented in Figures 9–11. The solid line in each figure has a slope of 1, and denotes the expected result for particles streaming along a uniform magnetic field in the absence of turbulence. The dashed line in each figure has a slope of $1/2$, and denotes the expected result for particles diffusing through a turbulent medium. The turnover exhibited by the data away from the solid line represents a transition to diffusion as the particles start to fully sample the tubulent structure of the field, for which $\Delta z_{\rm rms} \propto \sqrt{t}$. The dotted horizontal lines represent the values of the turbulence lengthscale s_T for each corresponding profiles (as noted in the figures).

We note that there is a good correlation between the turbulence lengthscale and distance that the ensemble of particles must traverse before transitioning from a streaming-like motion to a diffusion-like motion, though the turbulence lengthscales are somewhat smaller (by about a factor of 2) than the $\Delta z_{\rm rms}$ values at which the transition to diffusion occurs. This result indicates that relativistic particles with a radius of gyration R_g random walk through a turbulent field with a step-size that is approximately equal to the turbulence legthscale s_T of the underlying magnetic field (as defined by Γ and η in our

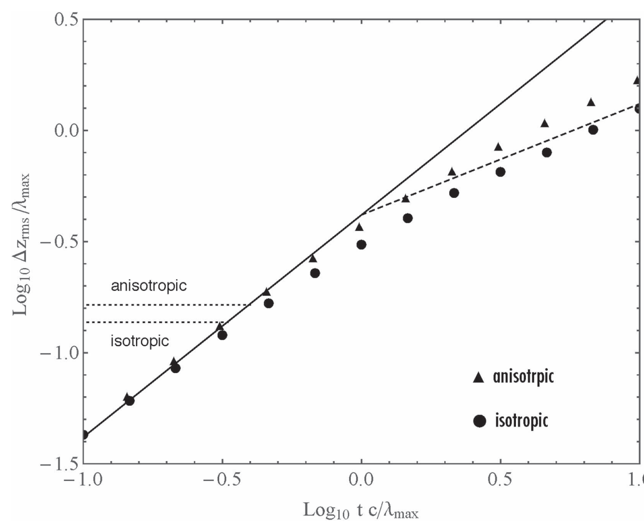

Figure 11. Root mean square values of the displacement Δz along the underlying field for an ensemble of particles injected into a turbulent magnetic field for both isotropic and anisotropic cases of profile 9 are poltted at the different times for which the distributions were calculated (with time given in terms of $c/\lambda_{\max}$). The solid line has slope 1 and the dashed line has slope $1/2$. The dotted horizontal lines represent the values of s_T for each case.

case) for which waves span over the range $\lambda_{\min} \approx R_g$ to $\lambda_{\max}$. Such information may prove useful to informing investigations that require a numerical approach to diffusion problems or seek to model diffusion using a simple random-walk approach.

5. Application to Molecular Clouds

Spanning tens of parsecs, giant molecular clouds (GMCs) contain $\sim 10^5 M_\odot$ of molecular gas distributed in a highly nonuniform, hierarchical structure characterized in terms of clumps ($R \sim 1$ pc, $n \sim 10^3$ cm^{-3}) and dense cores ($R \sim 0.1$ pc, $n \sim 10^4$–10^5 cm^{-3}) surrounded by an interclump gas of density $n \sim 5$–25 cm^{-3}.

While understanding the exact nature of the magnetic fields within GMCs remains a work in progress, significant advances have been made on both theoretical and observational fronts. With regard to global properties, an analysis of magnetic field strengths measured in molecular clouds yields a relation between the magnetic field strength B and particle number density n of the form

$$B \sim 10\ \mu\mathrm{G}\left(\frac{n}{10^2\ \mathrm{cm}^{-3}}\right)^{0.47}, \tag{12}$$

athough there is a significant amount of scatter in the data used to produce this fit (Crutcher 1999; but see also Basu 2000). This result is consistent with the idea that nonthermal linewidths, measured to be $\sim$1 km s^{-1} throughout the cloud environment (e.g., Lada et al. 1991), arise from MHD fluctuations. It is therefore generally believed that the magentic fields in GMCs are quite turbulent.

Advances in our understanding of turbulence within GMCs have benefitted greatly from numerical simulations (McKee & Ostriker 2007 and references therein) as well as new techniques for analyzing observations of Doppler broadened emission and absorption lines (Lazarian 2009). For example, a Velocity-Channel-Analysis applied to the full FCRAO Perseus map found a near Kolmogorov ($\beta = 5/3$) power-law turbulent energy spectrum $E(k) \propto k^{-\beta}$ with an exponent $\beta = 1.81 \pm 0.10$ (Padoan et al. 2006). More recently, a Velocity Coordinate Spectrum technique was applied to NGC 1333, also obtaining a power-law turbulent energy spectrum with a similar index $\beta = 1.85 \pm 0.04$ in the range $0.06\,\mathrm{pc} < l < 1.2\,\mathrm{pc}$ (Padoan et al. 2009). The absence of a turnover in the spectrum above the outflow energy injection lengthscale ($\approx$0.3 pc) seems to favor the scenario in which turbulence cascades from large-scales over one in which turbulence is internally driven by stellar outflows.

Such observational studies will be vital for our understanding of the sinks and sources of astrophysical turbulence, which in turn will aid in our understanding of MHD processes in such environments. For example, the smallest lengthscale over which magnetic fluctuations occur in GMC's remains poorly constrained. However, Alfvén waves can only couple to the neutral gas if the ion–neutral collision time $\tau_{ni} \approx (\langle\sigma v\rangle_{in} n_i)^{-1}$ is shorter than the MHD time (Mouschovias 1976; Shu 1983, 1992), where $\langle\sigma v\rangle_{in} \approx 1.7 \times 10^{-9}$ cm^{-3} s^{-1} is the average collision rate between ions and neutrals (Mouschovias 1991), and n_i is the number density of ions. As a result, magnetic disturbances with wavelengths shorter than $\lambda_{\rm crit} \equiv \pi v_\alpha \tau_{ni}$ diffuse before collisions between the neutrals and ions have had time to transmit to the neutrals the magnetic force associated with the disturbance (Mouschovias 1991; Balsara 1996). Since Alfvén waves become completely non-propagating and are quickly damped in this regime, we infer that $\lambda_{\rm min} = \lambda_{\rm crit}$. We adopt the scaling

$$n_i \approx 1.0 \times 10^{-4}\ \mathrm{cm}^{-3}\left(\frac{n}{10^2\ \mathrm{cm}^{-3}}\right)^{1/2}, \tag{13}$$

that follows if the ion density is set by the standard balance between recombination and cosmic-ray ionization at a rate $\zeta_{\rm CR} = 10^{-17}$ s^{-1} (Elmegreen 1979), but note thta this value can vary significantly (e.g., Fatuzzo et al. 2006). Assuming further a uniform Alfvén speed of $v_\alpha = 1$ km s^{-1} throughout the GMC environment, the minimum turbulence wavelengths are found to be $\lambda_{\rm min} \approx 1$–3 pc for the interclump medium, $\lambda_{\rm min} \approx 0.2$ pc for clumps, and $\lambda_{\rm min} \approx 0.02$–0.06 pc for cores.

It is reasonable to assume that the longest magnetic fluctuations correspond to the lengthscale over which they are generated. In the ISM, turbulence is generated by supernova remnants and stellar-wind collisions, so one might expect $\lambda_{\rm max}$ to be on the order of several parsecs (e.g., Coker & Melia 1997; Melia & Coker 1999). In this case, the range over which turbulence acts would vary from $d \lesssim 10$ in the interclump medium to $d \sim 10^4$ in dense cores. For the interclump medium, large amplitude ($\eta = 1$) Kolmogorov turbulence would have a turbulence lengthscale $s_T \sim 0.4\lambda_{\rm max}$ for both isotropic and anisotropic cases. At the other extreme, the corresponding turbulence lengthscale in dense cores would be $\sim 0.02\lambda_{\rm max} \sim 0.1$ pc. Given that the turbulence lengthscale in dense cores would then be comparable to the core radius, it's possible that turbulence becomes decoupled from physical processes that act within dense cores. This result may offer a possible explanation as to why oberved linewidths of dense cores are thermal (Myers & Fuller 1992).

Alternatively, it seems reasonable to assume that $\lambda_{\rm max}$ within a given structure (GMC, clump or core) cannot exceed the lengthscales that charaterize that structure, in which case one then finds that the dynamic range of turbulence throughout GMCs is $d \sim 10$. In turn, the turbulence lengthscale for large amplitude Kolmogorov turbulence would be $s_T \sim 0.4\lambda_{\rm max}$. Regardless of which of the two scenarios for setting $\lambda_{\rm max}$ holds for GMC environments, it appears that the turbulence lengthscale s_T is never much smaller than the size of the region in which that turbulence acts.

6. Conclusion

We have investigated the structure of turbulent magnetic fields through their Lyapunov coefficients. The turbulent magnetic field $\delta\boldsymbol{B}$ is calclauted by summing randomly oriented Alfvénic waves that logarithmically span wavevector space from $k_{\rm min} = 2\pi/\lambda_{\rm max}$ to $k_{\rm max} = 2\pi/\lambda_{\rm min}$, as developed by Giacalone & Jokipii (1994). A given profile of magnetic turbulence is specified through the three paramters Γ (powerindex), $d \equiv \lambda_{\max}/\lambda_{\min}$, and $\eta \equiv \langle \delta B \rangle^2 / B_0^2$, where B_0 represents the strength of an assumed uniform and static underlying magnetic field.

Ten magentic profiles are considered, as defined in Table 1. For profiles 1–3, Lyapunov exponents are calculated using several values of magnetic terms per decade as a means of establishing how many such terms are needed to adequately describe a continuous turbulent field via a discrete formalism. For profiles 1 and 8–10, both isotropic and anistotropic turbulence are considered. In each case, Lyapunov exponents are calculated for 200 realizations of each profile in order to build up meaningful distributions, and the mean $\langle \lambda_L \rangle$ and standard deviation σ_λ of each distribution is then used as the output measures that characterize the correspoding magnetic turbulence profile.

Our results indciated for large amplitude turbulence, 20 waves per decade provides a good approximation to the physical continuous turbulence magnetic field that is being modeled. Our results also show that there is a strong dependence between $\langle \lambda_L \rangle$ and each of the three profile parameters. Specifically, Lyapunov coefficients are larger for: (1) magnetic profiles whose wavelengths span a greater dynamic range as defined by d; (2) magnetic profiles for which magnetic intensity is spread out more equitably across the full range of wavelengths as specified by Γ, and (3) magnetic profiles with larger amplitude turbulence as defined by η.

Motivated by the fact that λ_L^{-1} represents the lengthscale over which neighboring fieldlines diverge, we define the turbulence lengthscale for a given profile as $s_T \equiv 1/\langle \lambda_L \rangle$, and show that this lengthscale correlates well to the distance cosmic rays must travel before transitioning from a streaming-like motion to a diffusion-like motion. The turbulence lengthscale can therefore be used to estimate the random-walk stepsize for diffusion problems, thereby informing numerical treatments of diffusion processes.

Finally, we apply our results to GMC environments, and find that the turbulence lengthscale s_T is never much smaller than the size of the region in which turbulence acts, and may offer a possible explanation as to why observed linewidths in dense cores are thermal.

We thank the referee for useful comments that greatly improved the manuscript. We also thank Dr. Fred Adams for useful discussions. M.F. is supported at Xavier University through the Hauck Foundation. Holden, Grayson and Wallace were supported by a 2012 Center for Integrative Natural Science and Mathematics (CINSAM) summer research grant.

References

Aharonian, F. A., & Atoyan, A. M. 1996, A&A, 309, 917
Atoyan, A. M., Aharonian, F. A., & Völk, H. J. 1995, PhRvD, 52, 3265
Balsara, D. S. 1996, ApJ, 465, 775
Basu, S. 2000, ApJL, 540, L103
Beresnyak, A. 2013, ApJL, 767, L39
Casse, F., Lemoine, M., & Pelletier, G. 2002, PhRvD, 65, 023002
Cho, J., & Lazarian, A. 2003, MNRAS, 345, 325
Cho, J., & Vishniac, E. T. 2000, ApJ, 539, 273
Coker, R. F., & Melia, F. 1997, ApJL, 488, L149
Crutcher, R. M. 1999, ApJ, 520, 706
Elmegreen, B. G. 1979, ApJ, 232, 729
Fatuzzo, M., Adams, F., & Melia, F. 2006, ApJL, 355, L49
Fatuzzo, M., & Melia, F. 2012, ApJ, 750, 21
Fatuzzo, M., & Melia, F. 2014, ApJ, 784, 131
Fatuzzo, M., Melia, F., Wommer, E., & Adams, F. 2010, ApJ, 725, 515
Giacalone, J., & Jokipii, J. R. 1994, ApJL, 430, L137
Goldreich, P., & Sridhar, S. 1995, ApJ, 438, 763
Jokipii, J. R. 1966, ApJ, 146, 480
Kulsrud, R., & Pearce, W. P. 1969, ApJ, 156, 445
Lada, E. A., Bally, J., & Stark, A. A. 1991, ApJ, 368, 432
Lazarian, A. 2009, SSRv, 143, 357
Lazarian, A., & Vishniac, E. T. 1999, ApJ, 517, 700
Lazarian, A., & Yan, H. 2014, ApJ, 784, 38
Lynn, J. W., Parrish, I. J., Quataert, E., & Chandran, B. D. G. 2012, ApJ, 758, 78
Lynn, J. W., Quataert, E., Chandran, B. D. G., & Parrish, I. J. 2013, ApJ, 777, 128
McKee, C., & Ostriker, E. 2007, ARA&A, 45, 565
Melia, F., & Coker, R. F. 1999, ApJ, 511, 750
Melia, F., & Coker, R. 1999, ApJ, 511, 750
Mouschovias, T. Ch. 1976, ApJ, 207, 141
Mouschovias, T. Ch. 1991, ApJ, 373, 169
Myers, P. C., & Fuller, G. A. 1992, ApJ, 396, 631
O'Sullivan, S., Reville, B., & Taylor, A. M. 2009, MNRAS, 400, 248
Padoan, P., Juvela, M., Kritsuk, A., & Norman, M. L. 2006, ApJL, 653, L125
Padoan, P., Juvela, M., Kritsuk, A., & Norman, M. L. 2009, ApJL, 707, L153
Shu, F. H. 1983, ApJ, 273, 202
Shu, F. H. 1992, Gas Dynamics (Mill Valley, CA: Univ. Science Books)
Wolf, A., Swift, J. B., Swinney, H. L., & Vastano, J. A. 1985, PhyD, 16, 285
Xu, S., & Yan, H. 2013, ApJ, 779, 140
Yan, H., & Lazarian, A. 2002, PhRvL, 89, 281102
Yan, H., & Lazarian, A. 2004, ApJ, 614, 757
Yan, H., & Lazarian, A. 2008, ApJ, 673, 942